Antiproton Interferometry and Aharonov-Bohm Effect (AIABE)

Andrey Alexandrov[1], Takashi Asada[2], Matias Bayo[3,4], Marco Beleggia[5], Fabrizio Castelli[6,4,†], Nicola D'Ambrosio[7], Giovanni De Lellis[8,1], Rafael Ferragut[3,4], Stefano Frabboni[5,9], Alberto Galanti[3,4], Gian Carlo Gazzadi[9], Marco Giammarchi[4,*], Vincenzo Grillo[9], Marco Leali[10,11], Giancarlo Maero[6,4], Valerio Mascagna[10,11], Simone Masci[7], Stefano Migliorati[10,11], Fabio Mombelli[10,11], Tatsuhiro Naka[2], Massimiliano Romé[6,4], Giovanni Roncoli[6,4], Valeri Tioukov[1], Valerio Toso[6,4] and Luca Venturelli[10,11]

1 INFN Sezione di Napoli, Italy
2 Department of Physics, Faculty of Science, Toho University, Japan
3 Politecnico di Milano, Italy
4 INFN Sezione di Milano, Italy
5 Università degli Studi di Modena and Reggio Emilia
6 Università degli Studi di Milano, Italy
7 INFN Laboratori Nazionali del Gran Sasso, Italy
8 Università degli Studi di Napoli Federico II
9 CNR-Istituto Nanoscienze, Modena, Italy
10 Dipartimento di Ingegneria dell'Informazione, Università degli Studi di Brescia, Italy
11 INFN Sezione di Pavia, Italy
* Correspondence: marco.giammarchi@mi.infn.it

Abstract: The Aharonov-Bohm (AB) effect is one of the most striking features of Quantum Physics, of critical importance to elucidate the role of the potential and its physical meaning. In spite of the fact that it was first proposed in 1946, up to now it was only demonstrated for electrons and neutrons. We propose the realization of an experiment to study the AB effect for the antiproton, which will have the double feature of being a non-elementary charged particle, and at the same time an antiparticle. The experiment will be conducted in collaboration with the ASACUSA group at the CERN AD (Antiproton Decelerator), making use of a slow antiproton beam.

Keywords: Aharonov-Bohm (AB) effect; Antimatter; Antiproton; Interferometry

1. Introduction

The Aharonov-Bohm (AB) effect is a quantum mechanical phenomenon by which a charged particle is affected by an electromagnetic potential in the same region where there is no electromagnetic field, and therefore no force in the classical sense. The concept was proposed, first according to the "gedanken" experimental scheme by Ehrenberg and Siday in 1949 [1], and then by Aharonov and Bohm in 1959 who highlighted the conceptual importance of the effect and how it could be used to assess the fundamental role played by the potential in Quantum Physics [2].

In its standard configuration the (magnetic) AB effect features a two-slits interference configuration, followed by a solenoid in a region where a particle beam is impinging on the system (fig. 1). In the ideal case the magnetic field outside the solenoid is zero while the vector potential **A** is non-zero; the relative phase of the two ideal wave functions (one per each *classical path*) is altered by an amount that depends on the magnetic field flux enclosed in the solenoid (Φ in fig. 1).

†Deceased

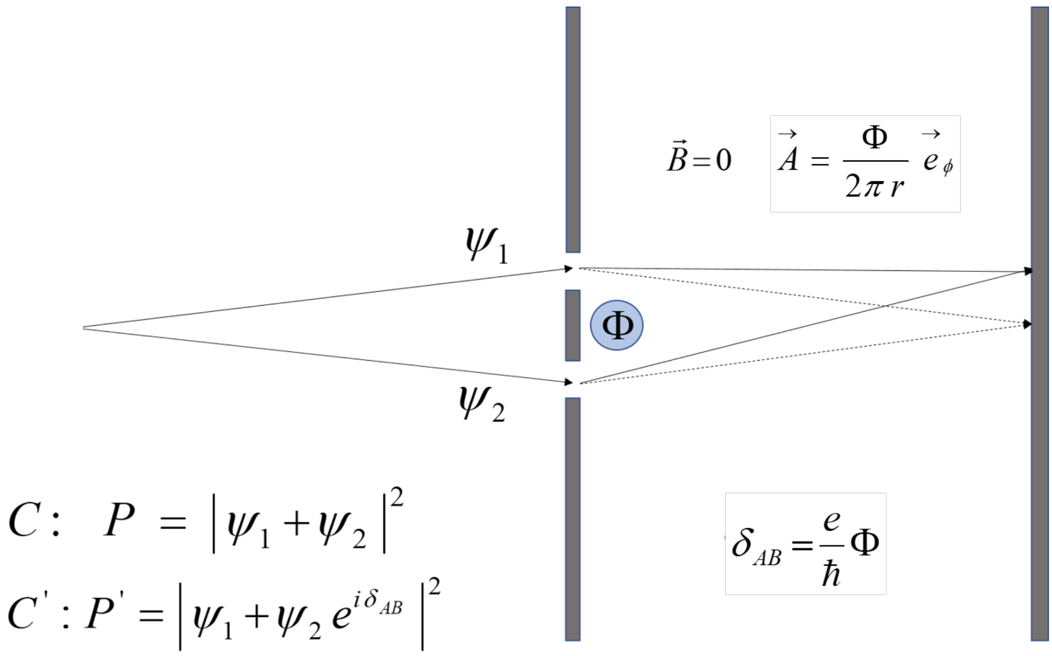

Figure 1. An example of the geometry for an experiment aimed at verifying the magnetic AB effect. With respect to the no-flux case (C), the presence of the magnetic flux Φ and the magnetic potential induces a phase shift (C') between the two wave functions 1 and 2. The two respective interference probabilities P and P' then differ by the AB phase factor δ_{AB}.

Even before its experimental demonstration, the AB effect generated a lively debate between theoreticians and experimentalists, thoroughly described in ref. [3], and prompted several experimental investigations, culminated with the 1986 experiment of Tonomura and colleagues [4]. This clear demonstration of the effect, obtained by excluding the magnetic field from the electron *classical path* with the help of a superconducting film, was then supplemented by additional experiments devoted to the verification of the "zero force" condition (see e.g. ref. [5]), a crucial characteristics of the effect.

In parallel with these developments, theoretical studies highlighted the connection of the AB effect with the concept of geometrical and topological phase of the Hilbert space underlying the physical quantum system (Berry's phase [6]). In addition, in 2016 the effect was demonstrated in the original "two slit" Ehrenberg-Siday configuration (as in fig. 1) by G. Pozzi and collaborators [7]; they made use of a uniformly magnetized bar with uniform cross section, whose effect is the same as the one of a straight "infinite" solenoid.

From the experimental point of view, in addition to the demonstration of the electric AB effect on electrons (see appendix A), studies were also made with a neutral particle, the neutron. In that case however, as illustrated in appendix B, the AB effect presents itself in the Aharonov-Casher form [23] (a magnetic moment flowing around a charged current) or of the scalar AB effect (with a pulsed magnetic field).

In spite of all this information, the magnetic AB effect for charged particles has only been demonstrated for a single elementary particle of the Standard Model: the electron. It has never been studied for any other particle and in particular never studied for a complex charged hadron, like the antiproton. In addition to being an antiparticle (adding to the interest of the study), the antiproton allows a new test of the CVC (Conserved Vector Current) concept, which can be considered as a new kind of test of the Ward-Takahashi identity [8,9].

One additional result of the experiment is the study of the dependence of the distribution with respect to the direction of magnetization (and the relative flux). In fact, a left-right asymmetry was found in a recent high-statistics AB experiment with electrons

[10], indicating a dependence on the sign of the magnetization. It was suggested that the effect could be due to a failure in the paraxial approximation normally used in Scattering Theory, as suggested by Shelankov [11] and further discussed by Berry [12].

The AB effect detection consists in the change of the quantum phase and therefore of the interference pattern produced by a grating configuration. Therefore the first part of this study will be the demonstration of the quantum interference of the antiproton, the second case for an antiparticle after the positron, demonstrated in 2019 [13].

2. Experimental Strategy

In order to study the AB effect with the antiproton, the realization of quantum interference is a necessary precondition. Given the mass of the particle, it is important to use a low energy beam, as the one that is available at the CERN ASACUSA experiment. In ASACUSA (Atomic Spectroscopy And Collisions Using Slow Antiprotons) antiprotons coming from the CERN accelerator system are trapped and cooled in the MUSASHI Penning-Malmberg trap [14]. This allows the subsequent formation of a slow antiproton beam with a kinetic energy of about 250 eV.

This slow antiproton beam has already been used in another experimental study [15] and, given its low energy, has a de Broglie wavelength of

$$\lambda_{dB} = h/mv \simeq 1.8\ pm \tag{1}$$

in the non-relativistic approximation. The beam has a velocity of 220,000 m/s and an intensity in the range of 2×10^3 particles/s, for an overall spill duration of 10 s. In these conditions the total statistical accumulation will be of 2×10^4 incoming antiprotons every 130 s, which is the repetition rate of the CERN Antiproton Decelerator machine seeding the ASACUSA setup [16].

The incoming antiprotons will be studied in a 1 m long interferometer, schematically shown in fig. 2. Given the beam velocity, the transit time will be of 5 μs and the mean particle arrival rate is around 100 μs^{-1}; therefore one can safely conclude that the experiment will work in single particle mode. This is another novelty of this approach with respect to the work done with electrons.

Detecting with good resolution an antiproton interference pattern is a prerequisite for the demonstration of the AB effect. For this reason, as a first step, we propose a Fraunhofer diffraction experiment according to the conceptual scheme presented in fig. 2.

Given the de Broglie wavelength under consideration, a 100 nm grating structure would diffract at 18 μm after a 1 m interference length. The detection therefore appears feasible with a very high resolution detector. For this reason, we propose the use of emulsion detectors, to be used as integrators of the diffraction signal. Emulsions films have a superior space resolution, in our case better than 1 μm [17,18] and they can detect the impact point of antiprotons by reconstruction of the relevant annihilation pions.

During the path traveled in the interferometer, the antiproton will be subjected to the Earth's magnetic field, which requires the presence of a mu-metal shielding. The deflection of a 250 eV antiproton traveling 1 m in the Earth magnetic field is of the order of 1 cm, which is reduced to only 10 μm by the kind of mu-metal we used in [13]. Moreover, one has to take into account that a constant magnetic field does not pose any problem and a factor 10^3 reduction will also reduce fluctuations accordingly.

Following the scheme of fig. 2, a first direct demonstration of antiproton interferometry can be obtained by a Fraunhofer interference-diffraction experiment with a material grating. A simulation was made assuming the use of a $N = 1000$ slits material grating, with single slit aperture of 200 nm and 10 μm inter-slit distance. Integrating over 10^6 detected antiprotons would produce the result schematized in fig. 3 (left), in terms of the interference

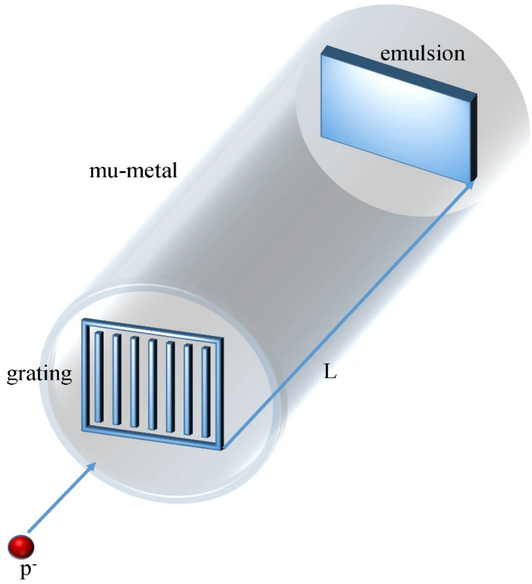

Figure 2. General scheme of the AIABE setup. The grating generates a diffraction pattern to be recorded in the emulsion detector. The system is 1 m long and will be enclosed in a mu-metal to mitigate the effect of the Earth's magnetic field.

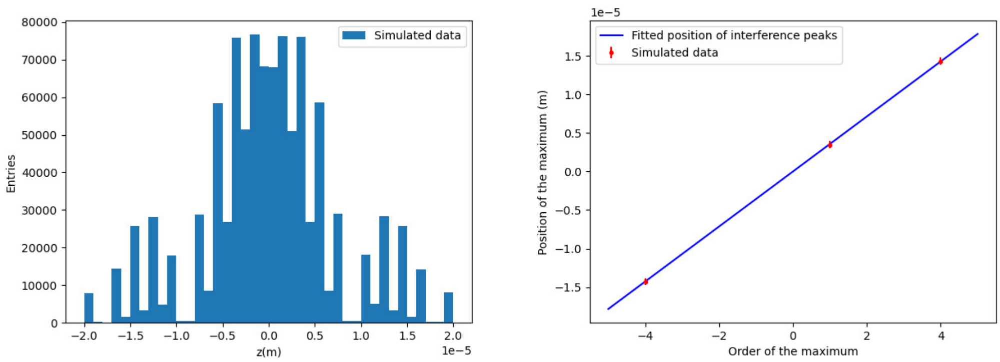

Figure 3. Simulation involving a 250 eV antiproton beam and a grating with $N = 1000$ slits, each having a 200 nm aperture and with an inter-slit distance of 10 μm. Left: distribution of the impact point on the detector. Right: least-square fit to the theoretical impact point distribution to obtain the de Broglie wavelength.

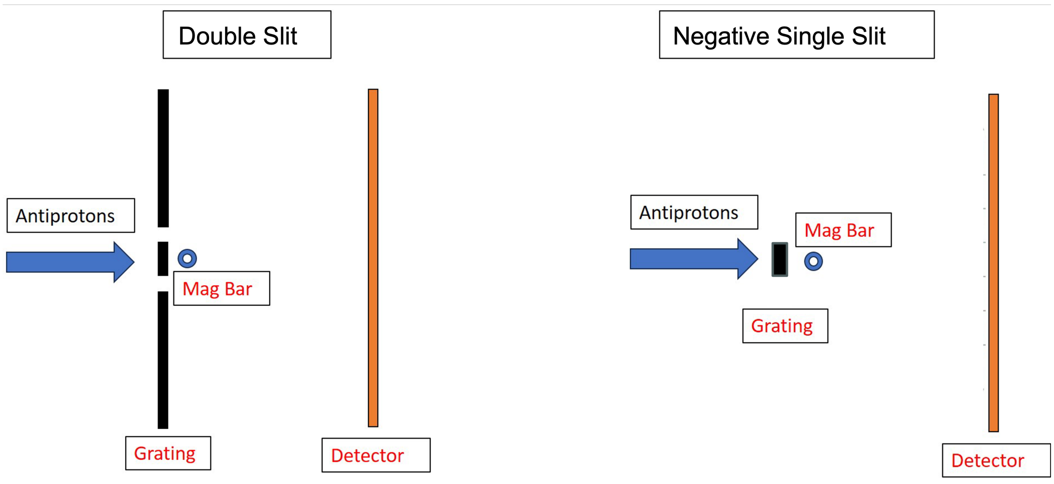

Figure 4. The configurations for the AB experiment. On the left hand side the classical configuration is shown, while on the right-hand side one can see a "negative" single block configuration which will give a similar interferometric result but with a much higher antiproton flux.

pattern on the emulsion. Given the geometric configuration, and the open fraction of the grating (about 2%), an amount of 5×10^7 impinging antiprotons are necessary to produce the pattern in figure, which is achievable with 3-4 days of data taking at the Antiproton Decelerator.

Once we have the demonstration of antiproton interferometry, the next logical path is the demonstration of the AB effect. This will be achieved following the conceptual scheme presented in fig. 4, where the classical double slit configuration as well as its anti-configuration are shown.

Under these conditions, the interference-diffraction of the 250 eV antiprotons would create a theoretical figure on the screen like the one shown in fig 5, where the difference between the two cases consists in a single unit of magnetic flux. The pattern of the minima and maxima are within the range of sensitivity of the emulsion detector even after 50 cm of propagation (red line in the figure).

In a configuration like this, let us suppose the use of the following (realistic) parameters:

- slit opening a = 250 nm;
- inter-slit distance of d = 1 μm for the double slit case;
- grating-detector distance of 1 m.

The working principle of the emulsion detector will be measuring the impact point (see figure 5) by the annihilation tracks coming from the pions. This technique relies on tracing, within the emulsion, the tracks produced by the annihilation of the antiproton. The 2-3 pions typically produced will leave distinct tracks that can be reconstructed as discussed in [17] and [18]. According to this reconstruction technique, the estimated error on the impact of the antiproton position will be of one micron.

However, the use of a classical two-slit configuration with material gratings will suffer the significant disadvantage of depressing the incoming antiproton flux. In addition, another important disadvantage is present: antiprotons stopped by materials generate pions, and that background can be important.

In order to overcome these problems, we will use a configuration like the one shown on the right hand side of fig. 4. The interferometric result by a configuration of this type is shown in the lower part of fig. 6. By contrast, the upper part of fig. 6 illustrates the case of no magnetic flux present.

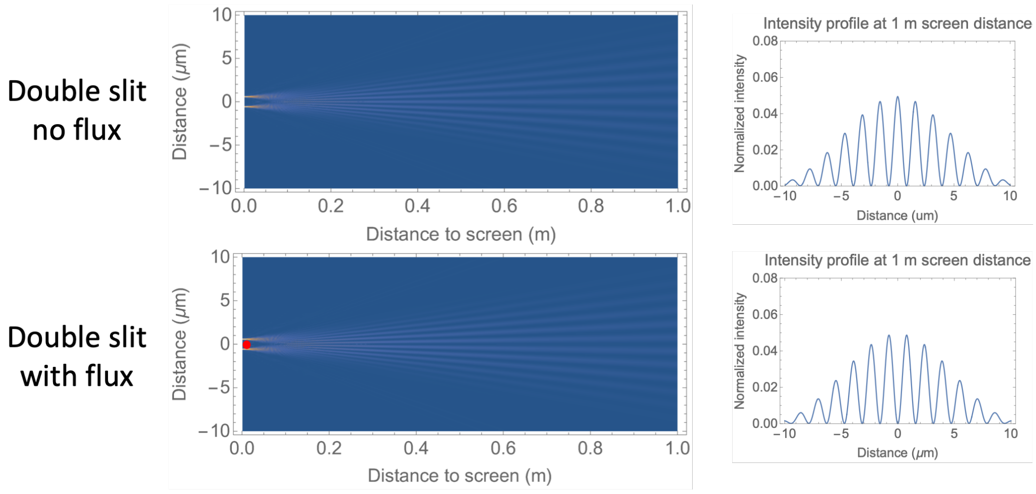

Figure 5. The interference and diffraction system generated by a two slit system under the condition on the left-side of 4, opening 500 nm, inter-slit distance 1 μm and 1 m distance from the detector/screen. The difference is of a single unit of magnetic flux $\hbar/e$ (red dot).

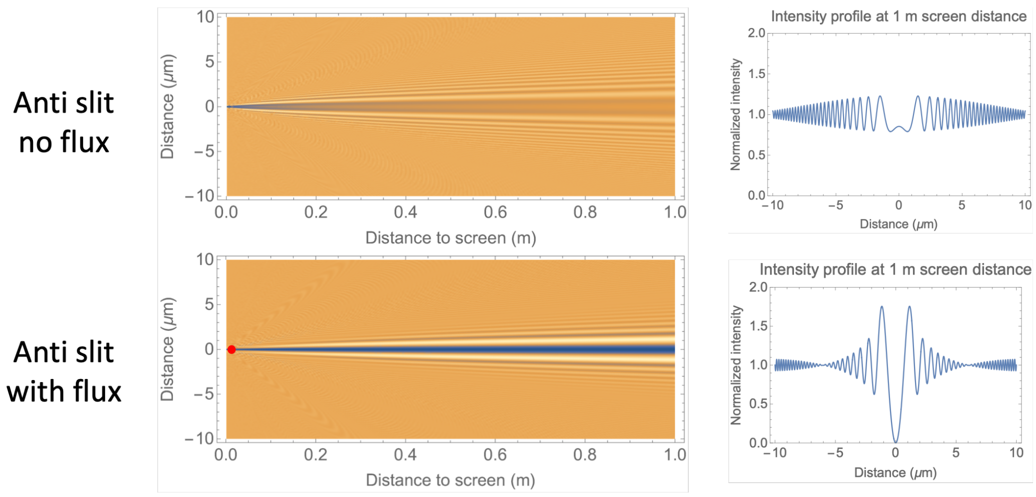

Figure 6. The configurations for the AB experiment would produce an interference and diffraction pattern indicated in figure, after propagation to the detector. The upper part refers to the presence of the obstacle alone (150 nm wide), while the lower part includes the magnetized bar generating one unit of magnetic flux $\hbar/e$ (red dot).

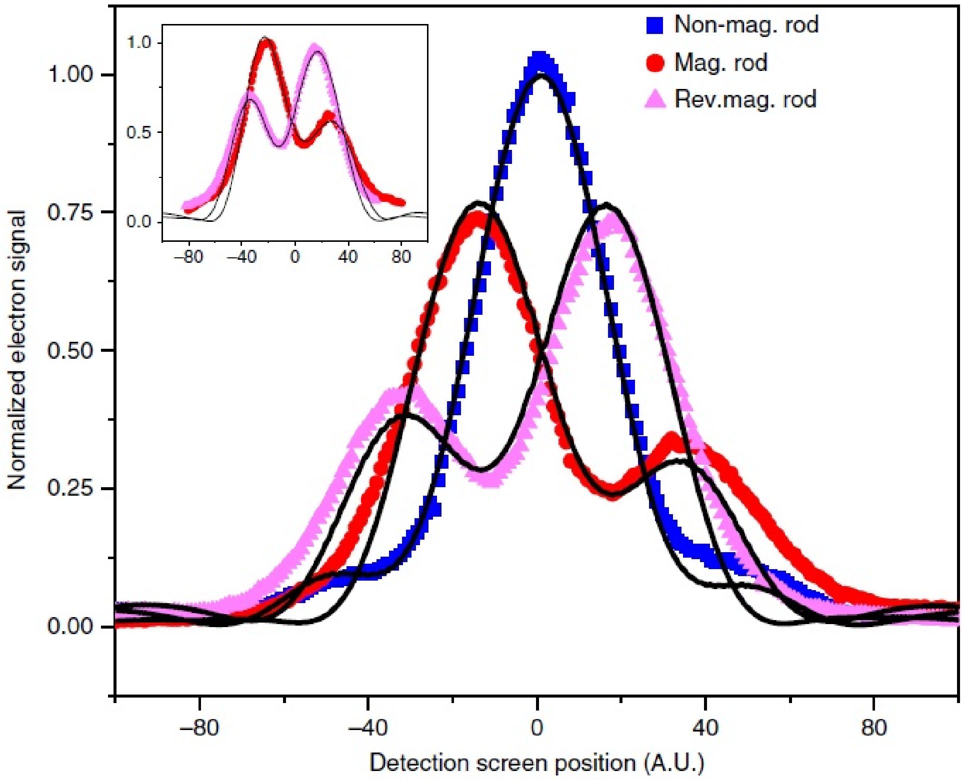

Figure 7. Symmetry reversal of the AB effect with electrons from the experiment in [10] with electrons. The AB effect shows here the two different signs obtained by rotating the magnetic rod by 180 degrees. Figure from ref. [10], reprinted with permission from the author.

As magnetic element we will use the bars developed for the AB experiment with electrons, as in [19] and [7]. Therefore, we propose a configuration like the one outlined on the right part of fig. 4, producing the interference pattern displayed in fig. 6.

The study of the magnetic AB-effect will be conducted by varying the angle of inclination of the magnetized bar, so that the amount of magnetic flux enclosed by the path of the particles can be changed in a continuous way.

The specific signature of the AB effect will be the asymmetry between the two cases of currents described in [10] and shown in figure 7, corresponding to a rotation of the magnetic bar by 180 degrees. In addition, all the intermediate rotation angles will be availables, including 90 degrees which produces the case of zero magnetic flux and provides a normalization of the effect.

3. Conclusion

We propose the exploration of antiproton interferometry in conjunction to the AB effect, by making use of the slow antiproton beam available at the ASACUSA setup in the CERN Antiproton Decelerator.

Acknowledgments: We would like to thank the ASACUSA Collaboration for considering the possibility of making this experiment in the frame of their experimental apparatus at CERN. This paper is dedicated to the memory of our colleague and co-author Fabrizio Castelli, who passed away during the preparation of this work. Finally, we also thank Herman Batelaan for useful discussions.

Conflicts of Interest: We do not have any conflicts of interest.

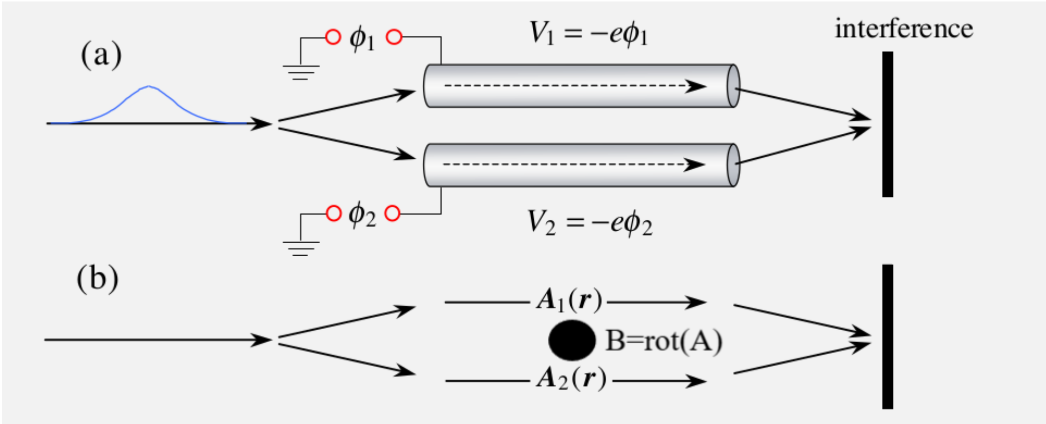

Figure A1. Figure (a) represents the so-called electric Aharonov-Bohm effect. After the wave packet has been splitted, the two parts pass in the region where V_1 and V_2 are different from zero. The electric field **E** is zero inside the cylinders (but not everywhere). Figure (b) represents the magnetic Aharonov-Bohm effect; again we split the wave packet in two and then we let it pass in a region where **A** is nonzero while $\mathbf{B} = 0$ due to the presence of an ideal solenoid. The only part where the magnetic field is nonzero is inside the solenoid.

Appendix A The Aharonov-Bohm effect

The Aharonov-Bohm effect refers to the quantum mechanical situation that arises when particles pass through regions where the potentials ϕ and **A** are nonzero, whereas the physical fields (electric field **E** and magnetic field **B**) are zero - and therefore no force is present in the classical sense.

For a charged particle, the wave function describing its dynamics can be expressed in such a way that the electromagnetic potentials ϕ and **A** appear in its phase. For example, an electron wave packet traveling in a region of potential energy $V = -e\phi$, acquires a phase $e\phi t/\hbar$. This follows directly from the Hamiltonian, which in this case is $H = p^2/2m - e\phi$. The AB effect in this case is shown in fig. A1 (a), where the wavefunction is *split* in two wave packets that (in the classical sense) will follow two different paths within two different conducting cylinders.

When the electron wave packets are inside the cylinders, one can turn on the potentials $V_1 = -e\phi_1$ and $V_2 = -e\phi_2$, which are switched off just before they leave the cylinders. The packets now have acquired a phase which is $e\phi_1\tau/\hbar$ and $e\phi_2\tau/\hbar$ (τ being the crossing time of the cylinders). Clearly, these two phases differ if $\phi_1 \neq \phi_2$. Now note that the electric field **E** acting on the packet classical path is always zero. Then, instead of experiencing **E** directly (and therefore a force), the particle is only subjected to the potential ϕ associated to **E**. The difference in the electrostatic potential of course has physical effects when the two wave packets are *recombined*; these effects were observed for the first time (demonstration of the electric AB effect) only in 1998 [20].

The situation in Fig. A1 (b) is similar in spirit but concerns the most common case of the magnetic AB effect. We split the wave packet into two separate wave packets, then let them pass in a region where there is a solenoid. Since the field is confined inside the solenoid, $\mathbf{A}_{1,2} \neq 0$ while $\mathbf{B} = 0$.

It is noteworthy that quantum mechanical waves are sensitive to potentials, which are not gauge-invariant quantities. Consider the gauge transformation $\mathbf{A} \to \mathbf{A} + \nabla\chi$, where χ is an arbitrary function of space and time. The wavefunction must change accordingly so that the transformation has no physical effect. This is one of the features that distinguishes classical particles from quantum particles.

In regions where $\mathbf{B} = 0$, to obtain the effect brought by **A** we only need to calculate a phase by integrating **A** over a convenient path. Consider the time dependent Schrödinger equation for a particle with charge q in a region where $\mathbf{B} = 0, \mathbf{A} \neq 0$, such as a path around the solenoid

$$i\hbar\frac{\partial \psi}{\partial t} = \frac{1}{2m}(-i\hbar\nabla - q\mathbf{A})^2\psi. \tag{A1}$$

The solution to this equation is given by the $\mathbf{A} = 0$ solution times a phase factor

$$\psi = \psi_0 e^{ig(\mathrm{r})} \;\; \text{with} \;\; g(\mathbf{r}) = (q/\hbar)\int_{\mathbf{r}_0}^{\mathbf{r}} \mathbf{A}(\mathrm{r}')\cdot d\mathrm{r}'.$$

In fact, inserting the solution in (A1) one has

$$(-i\hbar\nabla - q\mathbf{A})^2\psi = -\hbar^2(\nabla^2\psi_0)e^{ig(\mathbf{r})}.$$

This shows that the effect on the wave function caused by $\mathbf{A} \neq 0$ in a region where $\mathbf{B} = 0$ is accounted for by a phase factor.

The typical geometry for an experiment on the magnetic AB effect is the one shown in part b) of fig. A1. The $\mathbf{B}$ field (pointing outside of the page) is present only in the region inside the solenoid, while outside the cylinder $\mathbf{A} \neq 0$, so particles experience $\mathbf{A}$ but not $\mathbf{B}$. In the region where $r > a$, where a is the radius of the solenoid, we have;

$$\mathbf{A} = \frac{\Phi}{2\pi r}\hat{\phi},$$

where $\hat{\phi}$ points counterclockwise. Then, at the point of closest approach, the "lower" component of $\mathbf{A}$ points in the same direction of momentum of the wave packet, while the "upper" part points in the opposite direction; so phase shifts are introduced for both wave packets: in one case it *advances* the phase, in the other case it *delays* the phase.

Since the interference pattern depends on the phase, when we *recombine* the two packets we will see an effect due to the solenoid. We interpret this by saying that the vector potential $\mathbf{A}$ has a physical effect on the system. In fact, the presence of $\mathbf{A}$ results in a phase difference

$$\delta_{AB} = (q/\hbar)\left(\int_{\mathbf{r}_1}^{\mathbf{r}_2} d\mathbf{r}\cdot\mathbf{A}_{lower} - \int_{\mathbf{r}_1}^{\mathbf{r}_2} d\mathbf{r}\cdot\mathbf{A}_{upper}\right). \tag{A2}$$

Ee can reverse the limit of the second integral to obtain

$$\delta_{AB} = (q/\hbar)\oint d\mathbf{r}\cdot\mathbf{A}. \tag{A3}$$

By using Stokes' theorem we see that the phase difference δ_{AB} depends on the magnetic flux

$$\delta_{AB} = (q/e)\frac{\Phi}{\Phi_L}, \tag{A4}$$

with $\Phi_L \equiv \hbar/e$ the quantum of magnetic flux.

Appendix B The AB effect with neutrons

It is appropriate to briefly recall the main results obtained in the search for AB–type effects using neutrons. Since the neutron is electrically neutral, the standard magnetic and electric AB effects discussed in Appendix A are not directly applicable. However, the neutron possesses an intrinsic magnetic dipole moment $\boldsymbol{\mu}$ associated with its spin 1/2. This enables the occurrence of closely related quantum phase phenomena, which have been extensively investigated by neutron interferometry experiments [21].

In 1981, the group of Greenberger performed a neutron interferometry experiment explicitly designed to test the magnetic AB configuration with a solenoid, analogous to that used for charged particles [22]. No measurable phase shift was observed. The experiment set an upper bound showing that any AB phase for the neutron is smaller than about 5×10^{-12} of that for a particle with charge e. This result provided a stringent experimental confirmation that the magnetic AB effect is intrinsically linked to electric charge, and simultaneously constrained the possible electric charge of the neutron to extremely small values.

In 1984, Aharonov and Casher predicted that a neutral particle carrying a magnetic dipole moment should acquire a quantum phase when moving around a distribution of electric charge [23]. In this configuration, a neutron encircling a charged wire experiences no net classical force, yet its wave function acquires a non-dispersive phase

$$\varphi = \frac{1}{\hbar c^2} \oint d\mathbf{r} \cdot (\mathbf{E} \times \boldsymbol{\mu}), \tag{A5}$$

which ultimately depends only on the total charge enclosed by the trajectory, in close analogy with the magnetic AB effect for charged particles.

However, it is worth emphasizing an important conceptual difference. In the laboratory frame, the Aharonov–Casher (AC) phase can be interpreted as a geometric or topological effect. In the neutron rest frame, however, the electric field is transformed into an effective magnetic field that couples locally to the neutron magnetic moment, leading to a spin-dependent dynamical phase. The accumulated phase can therefore be viewed as arising from the integral of this local interaction along the path. This contrasts with the magnetic AB effect for charged particles, where the AB phase arises in the absence of any local gauge-invariant interaction term in the region accessible to the particle.

The first experimental verification of the AC effect was achieved in 1989 by Cimmino *et al.* using a neutron interferometer, observing a phase shift in quantitative agreement with the theoretical prediction [24].

A further development concerned the analogue of the electric (or scalar) AB effect for neutrons. Although neutrons are neutral, their magnetic moment implies a magnetic potential energy $U = -\boldsymbol{\mu} \cdot \mathbf{B}$. A neutron with spin parallel to a uniform static magnetic field undergoes a constant energy shift and, when traversing such a region, accumulates a phase without experiencing deflection or spin precession, in close analogy with an electron propagating in a region of constant electric potential.

In an interferometric configuration where a short magnetic-field pulse was applied synchronously to only one arm of the interferometer, a relative phase shift was observed in 1992 by Allman *et al.* [25], consistent with

$$\varphi = \frac{\mu}{\hbar} \int B(t)dt. \tag{A6}$$

That experiment employed an unpolarized neutron beam, consisting of two sub-populations with opposite spin orientation. Peshkin subsequently pointed out that, in this situation, the observed phase shift could in principle be interpreted as arising from the local interaction of the magnetic dipole with the time-dependent magnetic field (i.e., an ordinary Zeeman coupling), without the need to invoke a genuine AB-type mechanism [26].

A few years later the experiment was repeated by Lee *et al.* using a polarized neutron beam and an optimized setup [27]. In this case the scalar AB phase was observed in agreement with the predicted phase shift, exhibiting the expected linear dependence on the time integral of the magnetic field.

In summary, for neutrons both the Aharonov–Casher effect and the scalar AB analogue have been experimentally observed, whereas the standard magnetic AB effect is absent to very high precision. Unlike the case of charged particles, however, the physical interpretation of these neutron-induced phase shifts remains the subject of ongoing debate. Several authors emphasize that they can be entirely reduced to locally acting interactions between the neutron magnetic dipole moment and electromagnetic fields (in an appropriate reference frame), and therefore do not constitute a genuinely new topological effect [28]. Others, by contrast, stress that the observed phase shifts are coherent, non-dispersive quantum phenomena involving no net work performed on the particle, and thus share the defining characteristics of Aharonov–Bohm–type effects [29].

These considerations highlight the conceptual distinction between truly charge-based AB phases and their dipole-based analogues, and further motivates the interest in testing the magnetic AB effect with a massive, composite, charged particle such as the antiproton, as proposed in the present work.

Appendix C More on the physical meaning of the AB effect

As we have seen, the AB effect can be interpreted as the interaction with a potential (and not a classical field), indicating that the potentials have a more fundamental role in quantum physics. And of course while the value of $\mathbf{A}$ in the magnetic AB effect is gauge-dependent, the line-integral (the phase shift) is a gauge-invariant physical reality that affects the downstream interference pattern.

As clearly outlined in [21], a genuine effect *of the AB type* must have the typical signature of being independent from the particle velocity (kinetic energy). In fact, if the AB phase shift depended on the energy, the different components of the wave packet (having different velocities) would be affected in different ways, thereby deforming (or delaying) the wave packet - which is the typical action of a *force*. In fact the phase shift is independent of the energy or velocity of the particle, as was also demonstrated experimentally by Caprez [5].

This distinction between shift of the phase (without force) and shift of the wave packet (with an acting force) is the key difference between topological and dynamical effect in Quantum Physics.

References

1. Ehrenberg, W.; Siday, R. E.; The Refractive Index in Electron Optics and the Principles of Dynamics. *Proc. Phys. Soc.* **1949**, *B 62*, 8. https://doi.org/10.1088/0370-1301/62/1/303.
2. Aharonov, Y.; Bohm, D.; Significance of Electromagnetic Potentials in the Quantum Theory. *Phys. Rev.* **1959**, *115*, 485. https://doi.org/10.1103/PhysRev.115.485.
3. Olariu, S.; Popescu, I. I.; The quantum effects of electromagnetic fluxes. *Rev. Mod. Phys.* **1985**, *57*, 339. https://doi.org/10.1103/RevModPhys.57.339.
4. Tonomura, A.; Osakabe, N.; Matsuda, T.; Kawasaki, T.; Endo, J.; Evidence for Aharonov-Bohm effect with magnetic field completely shielded from electron wave. *Phys. Rev. Lett.* **1986**, *56*, 792. https://doi.org/10.1103/PhysRevLett.56.792.
5. Caprez, A.; Barwick, B.; Batelaan, H.; Macroscopic Test of the Aharonov-Bohm effect. *Phys. Rev. Lett.* **2007**, *99*, 210401. https://doi.org/10.1103/PhysRevLett.99.210401.
6. Berry, M. V.; Quantal Phase Factors Accompanying Adiabatic Changes. *Proc. R. Soc. Lond. Ser.* **1984**, *A 392*, 45. https://doi.org/10.1098/rspa.1984.0023.
7. Pozzi, G.; Boothroyd, C. B.; Tavabi, A. H.; Yücelen, E.; Dunin-Borkowski, R. E.; Frabboni, S.; Gazzadi, G. C.; Experimental realization of the Ehrenberg-Siday thought experiment. *Appl. Phys. Lett.* **2016**, *108*, 083108. https://doi.org/10.1063/1.4942462.
8. Ward, J. C.; An Identity in Quantum Electrodynamics. *Phys. Rev.* **1950**, *78*, 182. https://doi.org/10.1103/PhysRev.78.182.
9. Takahashi, Y.; On the generalized Ward Identify. *Il Nuovo Cimento* **1957**, *6*, 371. https://doi.org/10.1007/BF02832514.
10. Becker, M.; Guzzinati, G.; Béché, A.; Verbeeck, J.; Batelaan, H.; Asymmetry and non-dispersivity in the Aharonov-Bohm effect. *Nat. Comm.* **2019**, *10*, 1700. https://doi.org/10.1038/s41467-019-09609-9.
11. Shelankov, A. L.; Magnetic force exerted by the Aharonov-Bohm line. *Europhys. Lett.* **1998**, *43*, 623. https://doi.org/10.1209/epl/i1998-00408-4.
12. Berry, M. V.; Aharonov-Bohm beam deflection: Shelankov's formula, exact solution, asymptotics and an optical analogue. *J. Phys. A: Math. Gen.* **1999**, *32*, 5627. https://doi.org/10.1088/0305-4470/32/30/309.

13. Sala, S.; Ariga, A.; Ereditato, A.; Ferragut, R.; Giammarchi, M.; Leone, M.; Pistillo, C.; Scampoli, P.; First demonstration of antimatter wave interferometry. *Sc. Adv.* **2019**, *5*, eaav7610. https://doi.org/10.1126/sciadv.aav7610.
14. Kuroda, N; Torii, H. A.; Nagata, Y.; Shibata, M.; Enomoto, Y.; Imao, H.; Kanai, Y.; Hori, M., Saitoh, H.; Higaki, H.; Mohri, A.; Fujii, K.; Kim, C. H.; Matsuda, Y.; Michishio, K.; Nagashima, Y.; Ohtsuka, M.; Tanaka, K.; Yamazaki, Y.; Development of a monoenergetic ultraslow antiproton beam source for high-precision investigation. *Phys. Rev. Spec. Top.* **2012**, *15*, 024702. https://doi.org/10.1103/PhysRevSTAB.15.024702.
15. Amsler, C.; Breuker, H.; Bumbar, M.; Cerwenka, M.; Costantini, G.; Ferragut, R.; Fleck, M.; Giammarchi, M.; Gligorova, A.; Gosta, G.; Hunter, E. D.; Killian, C.; Kolbinger, B.; Kraxberger, V.; Kuroda, N.; Lackner, M.; Leali, M.; Maero, G.; Mascagna, V.; Matsuda, Y.; Migliorati, S.; Murtagh, D. J.; Nanda, A.; Nowak, L.; Rheinfrank, S.; Romé, M.; Simon, M. C.; Tajima, M.; Toso, V.; Ulmer, S.; van Beuzekom, M.; Venturelli, L.; Weiser, A.; Widmann, E.; Yamazaki, Y.; Zmeskal, J.; Antiproton annihilation at rest in thin solid targets and comparison with Monte Carlo simulations. *Eur. Phys. J. A* **2024**, *60*, 225. https://doi.org/10.1140/epja/s10050-024-01428-x.
16. Hunter, E. D.; Bumbar, M.; Amsler, C.; Bayo, M.; Breuker, H.; Cerwenka, M.; Costantini, G.; Ferragut, R.; Giammarchi, M.; Gligorova, A.; Gosta, G.; Hori, M.; Killian, C.; Kraxberger, V.; Kuroda, N.; Lanz, A.; Leali, M.; Maero, G.; Malbrunot, C.; Mascagna, V.; Matsuda, Y.; Migliorati, S.; Murtagh, D. J.; Romé, M.; Sheldon, R. E.; Simon, M. C.; Tajima, M.; Toso, V.; Ulmer, S.; Venturelli, L.; Weiser, A.; Widmann, E.; Optimizing antihydrogen production via slow plasma merging. *Phys. Plasmas* **2026**, *33*, 032119. https://doi.org/10.1063/5.0311707.
17. Ariga, A.; Ariga, T.; De Lellis, G.; Ereditato, A.; Niwa, K.; Nuclear Emulsions. In: Fabjan, C., Schopper, H. (eds) Particle Physics Reference Library. Springer, Cham. https://link.springer.com/chapter/10.1007/978-3-030-35318-6_9.
18. Alexandrov, A.; Buonaura, A.; Consiglio, L.; D'Ambrosio, N.; De Lellis, G.; Di Crescenzo, A.; Galati, G.; Lauria, A.; Montesi, M. C.; Tioukov V; Vladymyrov, M.; A new generation scanning system for the high-speed analysis of nuclear emulsions, *JINST* **2016**, *11*, P06002. https://doi.org/10.1088/1748-0221/11/06/P06002.
19. Gazzadi, G. C.; Mulders, H.; Trompenaars, P.; Ghirri, A.; Affronte, M.; Grillo V.; Frabboni, S.; Focused electron beam deposition of nanowires from cobalt tricarbonyl nitrosyl (Co(Co)3NO) precursor. *J. Phys. Chem. C* **2011**, *115*, 19606. https://doi.org/10.1021/jp206562h.
20. van Oudenaarden, A.; Devoret, M. H.; Nazarov, Yu. V.; Mooij, J. E.; Magneto-electric Aharonov–Bohm effect in metal rings. *Nature* **1998**, *391*, 768. https://doi.org/10.1038/35808.
21. Zeilinger, A.; Generalized Aharonov-Bohm Experiments with Neutrons. *Fundamental Aspects of Quantum Theory, NATO ASI Series* **1986**, *144*, 311. https://doi.org/10.1007/978-1-4684-5221-1_35.
22. Greenberger, D. M.; Atwood, D. K.; Arthur, J.; Shull, C. G.; Schlenker, M.; Is There an Aharonov-Bohm Effect for Neutrons? *Phys. Rev. Lett.* **1981**, *47*, 751–754. https://doi.org/10.1103/PhysRevLett.47.751.
23. Aharonov, Y.; Casher, A.; Topological Quantum Effects for Neutral Particles. *Phys. Rev. Lett.* **1984**, *53*, 319–321. https://doi.org/10.1103/PhysRevLett.53.319.
24. Cimmino, A.; Opat, G. I.; Klein, A. G.; Kaiser, H.; Werner, S. A.; Arif, M.; Clothier, R.; Observation of the topological Aharonov–Casher phase shift by neutron interferometry. *Phys. Rev. Lett.* **1989**, *63*, 380–383. https://doi.org/10.1103/PhysRevLett.63.380.
25. Allman, B. E.; Cimmino, A.; Klein, A. G.; Opat, G. I.; Kaiser, H.; Werner, S. A.; Scalar Aharonov–Bohm experiment with neutrons. *Phys. Rev. Lett.* **1992**, *68*, 2409–2412. https://doi.org/10.1103/PhysRevLett.68.2409.
26. Peshkin, M.; Comment on "Scalar Aharonov–Bohm experiment with neutrons". *Phys. Rev. Lett.* **1992**, *69*, 2017. https://doi.org/10.1103/PhysRevLett.69.2017.
27. Lee, W.-T.; Motrunich, O.; Allman, B. E.; Werner, S. A.; Observation of Scalar Aharonov–Bohm Effect with Longitudinally Polarized Neutrons. *Phys. Rev. Lett.* **1998**, *80*, 3165–3168. https://doi.org/10.1103/PhysRevLett.80.3165.
28. Peshkin, M.; Lipkin, H. J.; Topology, Locality, and Aharonov-Bohm Effect with Neutrons. *Phys. Rev. Lett.* **1995**, *74*, 2847–2850. https://doi.org/10.1103/PhysRevLett.74.2847.
29. Cimmino, A.; Allman, B. E.; Klein, A. G.; Kaiser, H.; Werner, S. A.; High precision measurement of the topological Aharonov–Casher effect with neutrons. *Nucl. Instrum. Methods Phys. Res. A* **2000**, *440*, 579–584. https://doi.org/10.1016S0168-9002(99)01040-2.